Carbon 114 (2017) 585–590

Contents lists available at ScienceDirect

Carbon

journal homepage: www.elsevier.com/locate/carbon

Direct growth of unidirectional spindle-shaped graphene nanoribbons on SiC

Yuping Jia [a, b], Liwei Guo [a, *], Jingjing Lin [a], Junwei Yang [a], Xiaolong Chen [a, **]

[a] Research & Development Center for Functional Crystals, Beijing National Laboratory for Condensed Matter Physics, Institute of Physics, Chinese Academy of Sciences, Beijing 100190, PR China
[b] State Key Laboratory of Luminescence and Applications, Changchun Institute of Optics Fine Mechanics and Physics, Chinese Academy of Sciences, 3888 Dongnanhu Road, Changchun 130033, PR China

ARTICLE INFO

Article history:
Received 5 September 2016
Received in revised form
7 December 2016
Accepted 17 December 2016
Available online 21 December 2016

ABSTRACT

Direct growth of self-aligned spindle-shape graphene nanoribbons (GNRs) on SiC(11-20) substrate is demonstrated. It is found all the GNRs are monolayer and one of edges of each endpoint of GNR is along direction of zigzag-edge. The length directions of the GNRs are all coincided with the [0001] direction of SiC due to the anisotropy surface energy of SiC. Furthermore, the doping type of GNRs is p-type and its carrier density is changing with the variation of ribbon width. The size-dependent Fermi level variation in sub-micron scale GNR renders a $P^-P^+P^-$ potential configuration in a single GNR. The existed zigzag edges and a special potential configuration in a single GNR make it promise for fabrication of graphene based devices as triode and spintronic device.

1. Introduction

Graphene-based nanostructures exhibit excellent electronic properties that are not present in extended graphene [1–4]. Oriented graphene nanoribbons (GNR) are commonly used as the basic unit for electronic device [5–7]. Therefore, controllable growth of the unidirectional GNRs are a premise to realize their applications. Usually, two traditional technique procedures for fabrication of GNRs are adopted, which are top-down [8–12] with the help of lithographic method and bottom-up [13,14] in terms of in-situ growth. However, lithography [8–10] brings about rough edges in the GNRs [15,16]. Although chemical vapor deposition (CVD) as one of bottom-up way has been used to grow oriented GNRs on Ge(001) [14], the GNRs are not single orientation but are randomly along two normal directions. And the GNRs on Ge(001) must be transferred to other insulation substrate to fabricate electronic devices due to the narrow bandgap of Ge. To overcome the shortcoming of the current techniques for GNRs, developing a method of direct growth of unidirectional GNRs on insulation substrate is desirable.

As well known, epitaxial graphene (EG) on SiC is compatible with the modern semiconductor procedure for graphene devices. It is expectable to grow graphene ribbons (GRs) on SiC in situ [17–20]. The GRs in micrometer scale in width grown on (11-20) oriented SiC (SiC(11-20)) [20] were reported. However, how to control the size of GRs is not concerned there, which is our focus. Here, we developed a two-step growth method on SiC(11-20), and GNRs with unidirectional alignment are achieved. The GNRs have special spindle-shape with widths 35–262 nm in their centers and 11–25 nm at their two endpoints. As a result of prominent width reduction of the ribbon from center to the endpoint, a $P^-P^+P^-$ potential configuration exists in a single ribbon along its length direction. These special properties of the GNRs on SiC(11-20) promise a potential applications in graphene based microelectronic and spintronic devices.

2. Experimental

The GNRs were in-situ grown on 6H-SiC(11-20) through thermal decomposition of SiC in a custom-built physical vapor transport (PVT) equipment. The surface morphology of a SiC(11-20) substrate is shown in Fig. S1. To obtain GNRs, a two-step growth process was designed: the step-I is a temperature-raise process and the step-II is a graphene growth process (as schematic shown in Fig. S2). In the step-I, growth temperature was raised from room temperature to about 1000 °C within 180 min under argon (Ar) gas protection in

* Corresponding author.
** Corresponding author.
E-mail addresses: lwguo@iphy.ac.cn (L. Guo), xlchen@iphy.ac.cn (X. Chen).

http://dx.doi.org/10.1016/j.carbon.2016.12.045
0008-6223/

pressure about 50 kPa. Then, the temperature was set to ramp to about 1500, 1600 and 1700 °C named as "growth temperature" within 15 min, correspondingly for Samples A, B and C. Because there is no temperature monitor equipment in our system, a true temperature does not know accurately. So an estimated temperature according to our experiences as illustrated in S2 is used. Simultaneously, the ambient pressure in growth system was lowered down rapidly from 50 kPa to 0.2–3 kPa by pumping. At the end of the step-II, the pressure was increased to 50 kPa immediately with filling Ar gas into the system. Then power was turned off, so that the further graphene growth was hindered. The detailed growth parameters concerning temperature and pressure are schematic shown in Fig. S2. In the whole process, the both of nucleation and evolution of GNRs happened in the step-II. It is found the size and density of GNRs can be well controlled through controlling the growth temperatures. The atomic force microscopy (AFM) (Bruker, Multimode 8) was used to characterize the morphology and the surface potential of GNRs samples. The Raman scattering instrument of HR800 was adopted to analyze layer number of GNRs, where a 532 nm laser focused to a spot in 1 μm diameter with a power 1 mW was used. The epitaxial orientation of graphene relative to SiC was drawn from analyzing transmission electron microscopy (TEM) diffraction pattern (the TEM instrument used here is Tecnat F20) on a continuous monolayer EG on SiC(11-20), which was perfectively developed from the GNRs such as Sample B by extending growth time.

3. Results and discussion

The AFM morphology images of Samples A, B and C are shown in Fig. 1(a)–(c). It is found that the GNRs are all self-similarity of a spindle-shape, and are all aligned along <0001> (C-axis) direction of SiC, no matter their sizes and densities. The density of GNRs rises with growth temperature increasing. They are $2.6 \times 10^7/cm^2$, $4 \times 10^7/cm^2$ and $5.2 \times 10^7/cm^2$ respectively for Samples of A, B and C as shown in Fig. 1(a)–(c). It can be seen in Fig. 1(a)–(c), the higher the growth temperature, the wider and longer the most of GNRs. The narrowest GNR in width about 35 nm is observed in Sample B as shown in Fig. 1(d), which was measured at position of its half-length (the center), while the width at the endpoint of the GNR is lowered down to 11 nm. Because of the spindle-shape, the width at the endpoint of a GNR can always be as small as 25 nm, although the center width is as large as 262 nm (as shown in Fig. S3). To determine the layer number of GNRs, the height profiles crossing the GNRs were measured as marked with color lines shown in Fig. 1(a)–(c). The sinkage depths of the GNRs relative to neighbor SiC are most in the range of 0.6 nm–0.7 nm as shown in Fig. 1(e)–(g), which is about 41% as the statistical analysis from 22 GNRs as shown in Fig. 2(a). Based on analysis, decomposition of each five Si-C single layers will form a monolayer of graphene with the same area and each of Si-C single layer of SiC(11-20) is in thickness of a/2 (a = 0.3073 nm). Considering the distance between graphene and SiC about 0.33 nm [21], the graphene thickness and the complex growth process of graphene, it is inferred that a sinkage depth of forming monolayer graphene should be around 0.7 ± 0.1 nm. A detailed analysis on this is given in supporting information S4. So, the most of GNRs obtained here should be monolayer according to the statistical results of Fig. 2(a). The inference is confirmed by analysis on Raman scattering spectra (Fig. 2(b) and Fig. S5). The Raman spectra randomly collected from GNRs in the three samples are shown in Fig. 2(b), where Raman signal from SiC was subtracted. The positions of 2D (G) peak for Samples of A, B and C are 2715 cm^{-1} (1601 cm^{-1}), 2706 cm^{-1} (1603 cm^{-1}), and 2703 cm^{-1} (1599 cm^{-1}) respectively. The narrow full width at half maximum (FWHM) of 2D peaks about 38 cm^{-1}, 37 cm^{-1} and 40 cm^{-1} and the high I_{2D}/I_G intensity ratio about 3.5, 1.9 and 3.2 for Samples A, B and C respectively suggest the GNRs are monolayer [22,23], which agrees well with the conclusion derived from sinkage depth profiles analysis. The clear D peaks in Raman spectra are due to the edges of GNRs. Besides the analysis on GNRs layer number, the width and length distribution as well as their aspect ratios were analyzed on 43 GNRs collected from Samples of A, B and C, as shown in Fig. 2(c) and (d). It is found that the widths of all the GNRs can be controlled smaller than 262 nm as supported

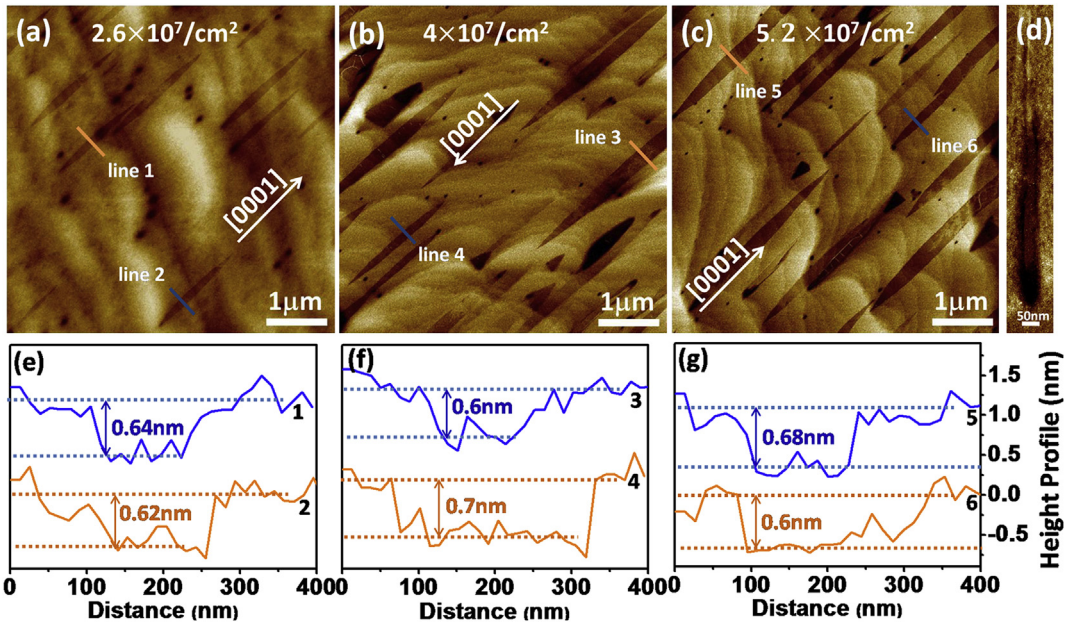

Fig. 1. AFM morphology images of Samples of A in (a), B in (b) and C in (c) respectively. The densities of GNRs in these three samples are expressed with the white numbers in their images. The morphology image of the narrowest GNR observed in Sample B is shown in (d). In Fig. 1(e)–(g), the height profiles of the marked GNRs with orange and blue lines are depicted under their images. (A colour version of this figure can be viewed online.)

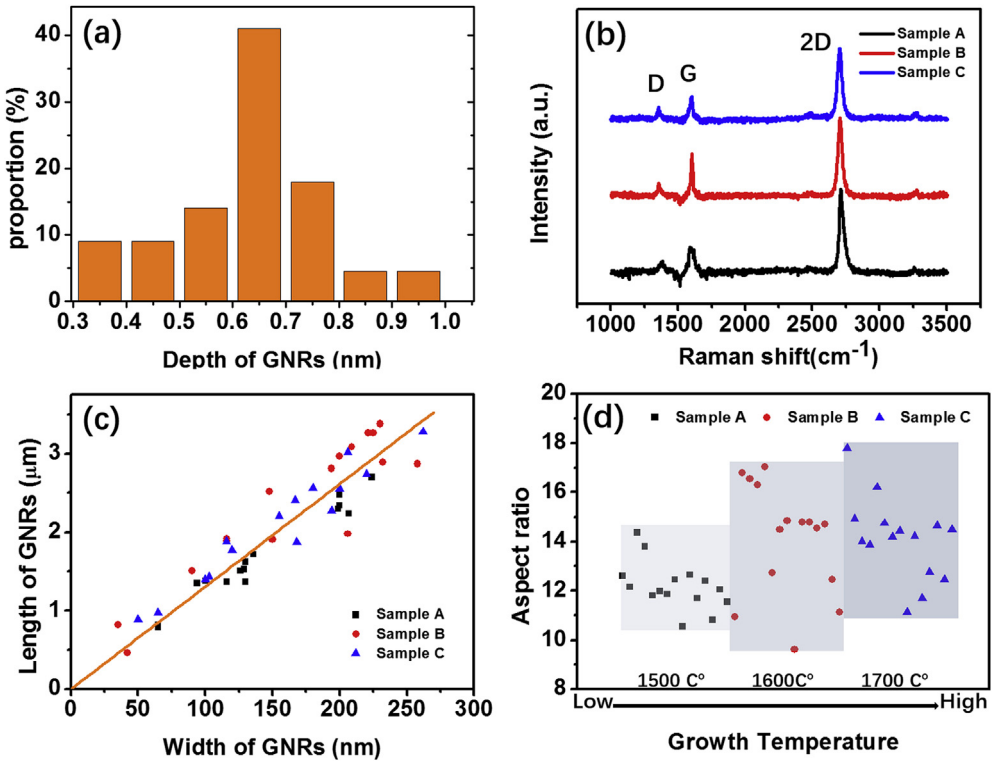

Fig. 2. Characterization on layer number and sizes of GNRs. (a) Histogram of the graphene sinkage depth proportion measured on 22 GNRs collected in the three samples. (b) Typical Raman spectra of GNRs in the samples after subtracting the Raman signal from SiC. (c) and (d) are distributions of width and length of GNRs, and their aspect ratios. (A colour version of this figure can be viewed online.)

by Fig. 2(c), and the average aspect ratio is around 13 for the GNRs on the three samples as manifested by the slope of the fitting line in Fig. 2(c). That indicates the influence of growth temperature is insignificant on the aspect ratio itself, but is prominent on the aspect ratio dispersion degree as shown in Fig. 2(d).

The observation of unidirectional orientation of GNRs suggests that the EG on the SiC(11-20) must have an inherent orientation relation with respect to SiC(11-20) substrate. To reveal the crystallographic orientation of graphene on SiC(11-20), a plane view TEM was performed on a continuous monolayer EG grown on SiC(11-20). The unique one set of hexagonal symmetry diffraction pattern coming from graphene, as partly sketched with red dot lines in Fig. 3(a), suggested that the graphene is monolayer or multilayers with the same orientation. However, the possibility of multilayer graphene is excluded as explained in S6. Meanwhile, the diffraction reveals the orientation relation between graphene and SiC. The yellow dot line is a guide for SiC <0001> direction (C-axis). It is found the armchair direction of GNR is rotated 21° with respect to the <0001> direction of the SiC. The orientation relation between the basic vectors of graphene (red arrows) and SiC(11-20) (black arrows) are shown in Fig. 3(b), where the red dashed line direction is along armchair direction of GNR. To reveal the edge structures of the GNR, the angle values of two sharp endpoints of GNRs were statistically analyzed as shown in Fig. S7. The angles of the GNRs edges relative to C-axis of SiC are labeled as α, β for one endpoint, γ and δ for another respectively. It is found that the values of angles β and γ are almost 9°. Concurrently the ∠(α+β) is always smaller than ∠(γ+δ) in the same GNR. Furthermore, it is determined that the terminal endpoint composed of angle (α+β) is always pointing to the [0001] direction of SiC, while the other endpoint composed of angle (γ+δ) is pointing to the [000-1] direction. The conclusion is deduced by identifying the polar of the {0001} planes of the used SiC(11-20) substrate by etching the SiC polar plane with molten potassium hydroxide. A detailed analysis is given in S8. According to the orientation relation between the EG and SiC as shown in Fig. 3(a), together with the angle values of β and γ, it is deduced that the edges of GNR constructing angles of β and γ are along the direction of zigzag-edge as schematically shown in Fig. 3(c). That means the most parts of the edges may be zigzag edges, although there may exist some irregular parts. The spin states in zigzag edges at the narrow terminal ends are interesting for exploring novel properties for graphene spintronics [4] to need studying in-depth.

The reason of direct growth of unidirectional GNR on SiC(11-20) is ascribed to the anisotropy growth rate of graphene, which is considered to be driven by the anisotropy surface energy of SiC. On a SiC(11-20) surface, there may exist irregular steps or kinks due to miscut along [11-20] crystal axis. The steps or kinks are usually composed of facets of {0001} or {10-10} facets. It is known that surface energies of (10-10), (0001) and (000-1) planes of SiC are to be 3.36 J/m^2, 2.20 J/m^2 and 0.30 J/m^2 respectively [24,25]. The smaller surface energy means the large distance between the adjacent planes and the lower density of dangling bonds on the exposed surface. Therefore, the atoms at the kinks or steps with low surface energy are tending to decomposition first at high temperature. That means Si-C atoms on the {0001} facets decomposed first, so a fast evolution of graphene along C-axis direction happened and a graphene ribbon with its length direction along C-axis of SiC is developed. Because the decomposition rate on (000-1) facet is faster than on (0001) facet due to even lower surface energy of SiC (000-1) plane, a faster graphene growth towards [0001] direction happened with the retreat of SiC (000-1) facets. Thus an even smaller terminal angle pointing to [0001] direction is resulted as shown in Fig. 3(c). Furthermore, the surface energy of (10-10)

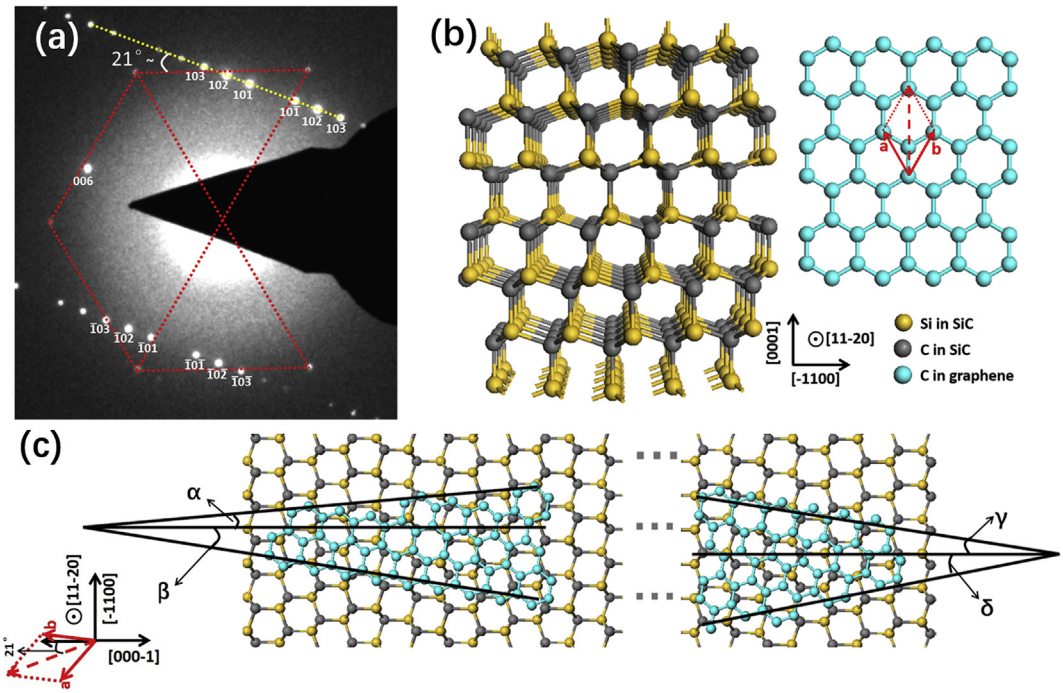

Fig. 3. Epitaxial orientation relation of GNR with respect to SiC, as well as the edge structure of GR. (a) TEM diffraction patterns of EG on SiC(11-20). (b) Schematic illustration of structures of 6H SiC and graphene, and their relative orientations, where the red (black) arrows are vectors of graphene (SiC). (c) Schematic edge structures of GNR near the terminal ends. The angles constructed by the edges of GNR and the C-axis of SiC at the two ends are marked as α, β, γ and δ, where angles of α+β and γ+δ are pointing to [0001] and [000-1] directions respectively, and two edges constructing angles of β and γ are along the direction of zigzag-edge. (A colour version of this figure can be viewed online.)

facet is more than ten times of that of (000-1), so that growth rate of graphene along <0001> direction is more than ten times of that along <10-10> direction, which is supported by a large aspect ratio (about 13) of GNR as shown in Fig. 2(d).

Usually a substrate offers doping effect on graphene [26]. To make sure the carrier type of GNRs on SiC(11-20), the AFM in an electrically biased tapping mode (eb-TM) is adopted as shown in supporting information S9 [27,28]. A p-type carriers was deduced in the GNRs, distinguished from that a continuous graphene on SiC(11-20) with a n-type doping [21]. Besides carrier type, the Fermi level of graphene is also important for electronic device. To explore Fermi level of GNR, surface potential was adopted and measured using Kelvin Probe Force Microscopy (KPFM). Sample C as a representative was measured. Contact potential difference (V_{CPD}) between the tip of KPFM and the surface of a sample is used as the detecting signal (detailed defined is given in supporting information S10). Fig. 4(a) shows the V_{CPD} mapping. A magnified local mapping of the V_{CPD} in the rectangle area outlined by yellow line is shown in Fig. 4(b). Here the V_{CPD} values of GNR and SiC are expressed as $V_{CPD\text{-}GNR}$ and $V_{CPD\text{-}SiC}$ respectively. It is found that the $V_{CPD\text{-}GNR}$ is obviously larger than the $V_{CPD\text{-}SiC}$. The larger V_{CPD} corresponds to a larger work function as well as a lower Fermi level. As schematically illustrated in inset of Fig. 4(b), the work function of GNR is larger than the work function of SiC, so that Fermi level of GNR is lower than that of SiC. Fig. 4(c) gives a statistically analysis on the contact potential difference ($V_{CPD\text{-}GNR}$ -$V_{CPD\text{-}SiC}$) between the

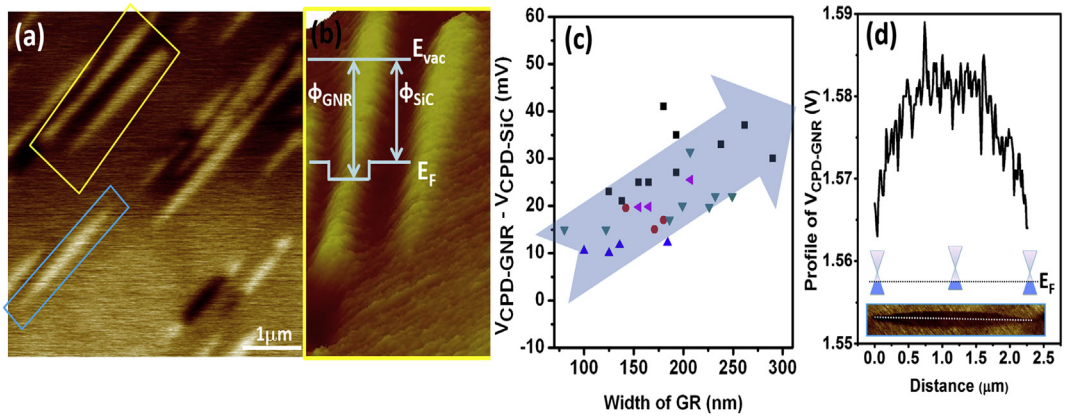

Fig. 4. The surface potential analysis of Sample C. (a) Surface potential mapping. (b) A magnified mapping in area of a yellow line outlined rectangle area in (a). (c) The values of ($V_{CPD\text{-}GR}$ -$V_{CPD\text{-}SiC}$) from five different regions in Sample C distinguished with different symbols and colors. (d) The $V_{CPD\text{-}GNR}$ along a single GNR. The bottom insets are morphology image of the GNR marked in (a) with a rectangle outlined by blue line and the schematic band structure at the three corresponding positions of the morphology image. (A colour version of this figure can be viewed online.)

GNRs and SiC, where the data are coming from 28 GNRs in five different regions of Sample C. Quantitatively, the Fermi level difference between the GNR and SiC is about 10–40 meV. As Fermi level of semi-insulate 6H-SiC is located in middle of its band gap about 4.95 eV [29], therefore the Fermi level of GNR should be in the range of 4.96 eV–4.99 eV. Because the Dirac point of intrinsic graphene is about 4.5 eV lower than the vacuum level [30], the Fermi level of GNR on SiC(11-20) is below Dirac point of 0.46 eV–0.49 eV, so that a p-type doped GNR is derived. The conclusion agrees well with the inference deduced from eb-TM analysis mentioned above. Noticeably, it can be clearly seen that ($V_{CPD\text{-}GNR}$ -$V_{CPD\text{-}SiC}$) shows increasing tendency with GNR's width widening. As $V_{CPD\text{-}SiC}$ is nearly a constant if considering the SiC is uniform, it is inferred that $V_{CPD\text{-}GNR}$ increases with width of GNR increasing. That means the Fermi level of GNR will lower down with width of GNR increasing. The $V_{CPD\text{-}GNR}$ profile along length of a single GNR is show in Fig. 4(d), where the same variation rule of $V_{CPD\text{-}GNR}$ versus the width of GNR is observed. The $V_{CPD\text{-}GNR}$ at the narrow ends is smaller than that in the center, which is a common phenomenon in our GNRs as show in supporting information S11. This variation of work function along the length provides an inherent $P^-P^+P^-$ potential configuration, which is analogous to a NPN configuration, in one single GNR as depicted in a schematic band structure in the inset of Fig. 4(d).

The clear Fermi level variation with width of GNR is well studied and reported both in theory and experiments [1–3], where quantum confinement of size effect is the dominant causes to lead to the variation of Fermi level and even to open a gap. However, the center width of our GNR is too wide over several tens nanometers to open a band gap. Thus, Fermi level variation here is due to other reasons, such as decorations on GNR edges in the air atmosphere. It is clear that the unbinding atomic density on the edges of a narrow GR is higher compared with that of a wider one, so the adsorption especially the polar molecules as H_2O is more considerable, which provides more free electrons to graphene [31], resulting in a higher Fermi level. On the other hand, comparing with the fresh samples just after growth, Fermi levels of the stale samples become even higher because the adsorption at edges become severer after exposed in air for a long time (as shown in supporting information S12). These two phenomena both support that the Fermi level upshift is a result of the adsorption on edges of GNR. That indicates the higher edge density is responsible to the observed higher Fermi level in a narrower GNR. Hence, Fermi level of GNR can be modulated via changing the width of GNR in the sub-micrometer scales. If GNR is decorated by special molecule, the variation of its Fermi level will become serious. Thus, our experimental results provide a new way for adjusting Fermi level of graphene ribbon.

4. Conclusion

Controllable fabrication of spindle-shaped monolayer GNRs were realized on the SiC(11-20) by two-step growth method developed here. The GNRs are self-aligning along the C-axis of SiC with their smaller terminal angle pointing to [0001] direction and each terminal end has at least one edge along the direction of zigzag-edge. The narrowest width of GNR in center is as small as 35 nm, and the width at the terminal ends of the most of GNRs are narrower than 25 nm. Furthermore, the Fermi level of GNR can be modulated through changing width of GNR and an inherent $P^-P^+P^-$ potential configuration is observed in one single GNR. Our spindle-shape GNR with edges along zigzag-edge direction combined with the special potential configuration will provide potential advantages for fabrication of graphene triode or spintronic devices.

Acknowledgments

This work is partly supported by the grants from the National key Basic Research Program of China (Nos 2013CBA01603), and the National Natural Science Foundation of China (Nos 51472265 and 51272279).

Appendix A. Supplementary data

Supplementary data related to this article can be found at http://dx.doi.org/10.1016/j.carbon.2016.12.045.

References

[1] Melinda Y. Han, Barbaros Özyilmaz, Yuanbo Zhang, Philip Kim, Energy band-gap engineering of graphene nanoribbons, Phys. Rev. Lett. 98 (2007) 206805.
[2] Y.Y. Li, M.X. Chen, M. Weinert, L. Li, Direct experimental determination of onset of electron-electron interactions in gap opening of zigzag graphene nanoribbons, Nat. Commun. 5 (2014) 4311.
[3] Verónica Barone, Oded Hod, Gustavo E. Scuseria, Electronic structure and stability of semiconducting graphene nanoribbons, Nano Lett. 6 (2006) 2748.
[4] Gábor Zsolt Magda, Xiaozhan Jin, Imre Hagymási, Péter Vancsò, Zoltán Osváth, Péter Nemes-Incze, et al., Room-temperature magnetic order on zigzag edges of narrow graphene nanoribbons, Nature 514 (2014) 608.
[5] Stefano Borini, Richard White, Di Wei, Michael Astley, Samiul Haque, Elisabetta Spigone, et al., Ultrafast graphene oxide humidity sensors, ACS Nano 7 (2013) 11166.
[6] Yu-Ming Lin, Alberto Valdes-Garcia, Shu-Jen Han, Damon B. Farmer, Inanc Meric, Yanning Sun, et al., Wafer-scale graphene integrated circuit, Science 332 (2011) 1294.
[7] Fengnian Xia, Damon B. Farmer, Yu-ming Lin, Phaedon Avouris, Graphene field-effect transistor with high on/off current ratio and large transport band gap at room temperature, Nano Lett. 10 (2010) 715.
[8] Esteban Climent-Pascual, Miguel García-Vélez, Ángel Luis Álvarez, Carmen Coya, Carmen Munuera, Xavier Díez-Betriu, et al., Large area graphene and graphene oxide patterning and nanographene fabrication by one-step lithography, Carbon 90 (2015) 110.
[9] Won Mook Choi, Tran Van Tam, Nguyen Bao Trung, Fabrication of sub-micrometer graphene ribbon using electrospun nanofiber, J. Mater. Sci. 49 (2014) 1240.
[10] Narendra Kurra, Abhay A. Sagade, Giridhar U. Kulkarni, Ultrafast direct ablative patterning of HOPG by single laser pulses to produce graphene ribbons, Adv. Funct. Mater. 21 (2011) 3836.
[11] Sridhar Vadahanambi, Jung-Hwan Jung, Rajesh Kumar, Hyun-Jun Kim, Il-Kwon Oh, An ionic liquid-assisted method for splitting carbon nanotubes to produce graphene nano-ribbons by microwave radiation, Carbon 53 (2013) 391.
[12] Liying Jiao, Xinran Wang, Georgi Diankov, Hailiang Wang, Hongjie Dai, Facile synthesis of high-quality graphene nanoribbons, Nat. Nanotechnol. 5 (2010) 321.
[13] Timothy H. Vol, Mikhail Shekhirev, Donna A. Kunkel, Martha D. Morton, Eric Berglund, Lingmei Kong, et al., Large-scale solution synthesis of narrow graphene nanoribbons, Nat. Commun. 5 (2014) 3189.
[14] Robert M. Jacobberger, Brian Kiraly, Matthieu Fortin-Deschenes, Pierre L. Levesque, Kyle M. McElhinny, Gerald J. Brady, et al., Direct oriented growth of armchair graphene nanoribbons on germanium, Nat. Commun. 6 (2015) 8006.
[15] E.R. Mucciolo, A.H. Castro Neto, C.H. Lewenkopf, Conductance quantization and transport gaps in disordered graphene nanoribbons, Phys. Rev. B 79 (2009) 075407.
[16] Karri Saloriutta, Y. Hancock, Asta Kärkkäinen, Leo Kärkkäinen, Martti J. Puska, Antti-Pekka Jauho, Electron transport in edge-disordered graphene nano-ribbons, Phys. Rev. B 83 (2011) 205125.
[17] M.S. Nevius, F. Wang, C. Mathieu, N. Barrett, A. Sala, T.O. Mentes, A. Locatelli, E.H. Conrad, The bottom-up growth of edge specific graphene nanoribbons, Nano Lett. 14 (2014) 6080.
[18] F. Wang, G. Liu, S. Rothwell, M.S. Nevius, C. Mathieu, N. Barrett, A. Sala, T.O. Mentes, A. Locatelli, P.I. Cohen, et al., Pattern induced ordering of semi-conducting graphene ribbons grown from nitrogen-seeded SiC, Carbon 82 (2015) 360.
[19] Nicolas Camara, Antoine Tiberj, Benoit Jouault, Alessandra Caboni, Bilal Jabakhanji, Narcis Mestres, et al., Current status of self-organized epitaxial graphene ribbons on the C face of 6H-SiC substrates, J. Phys. D. Appl. Phys. 43 (2010) 374011.
[20] Alessandra Caboni, Nicolas Camara, Esther Pausas, Narcis Mestres, Philippe Godignon, Nanobaguettes single epitaxial graphene layers on SiC(11-20), Mater. Sci. Forum 679–680 (2011) 781.
[21] M. Ostler, I. Deretzis, S. Mammadov, F. Giannazzo, G. Nicotra, C. Spinella, et al., Direct growth of quasi-free-standing epitaxial graphene on nonpolar SiC surface, Phys. Rev. B 88 (2013) 085408.

[22] Dong Su Lee, Christian Riedl, Benjamin Krauss, Klaus von Klitzing, Ulrich Starke, Jurgen H. Smet, Raman spectra of epitaxial graphene transferred to SiO_2, Nano Lett. 8 (2008) 4320.
[23] D. Graf, F. Molitor, K. Ensslin, C. Stampfer, A. Jungen, C. Hierold, L. Wirtz, Spatially resolved raman spectroscopy of single- and few-layer graphene, Nano Lett. 7 (2007) 238.
[24] Takayuki Narushima, Andreas M. Glaeser, High-temperature morphological evolution of lithographically introduced cavities in silicon carbide, J. Am. Ceram. Soc. 84 (2001) 921.
[25] Tsunenobu Kimoto, Akira Itoh, Hiroyuki Matsunami, Step bunching in chemical vapor deposition of 6H- and 4H-SiC on vicinal SiC(0001) faces, Appl. Phys. Lett. 66 (1995) 3645.
[26] R. Yang, Q.S. Huang, X.L. Chen, G.Y. Zhang, H.J. Gao, Substrate doping effects on raman spectrum of epitaxial graphene on SiC, J. Appl. Phys. 107 (2010) 034305.
[27] Lili Jiang, Bin Wu, Hongtao Liu, Yuan Huang, Jianyi Chen, Dechao Geng, et al., A general approach for fast detection of charge carrier type and conductivity difference in nanoscale materials, Adv. Mater. 25 (2013) 7015.
[28] Yuping Jia, Liwei Guo, Zhilin Li, Jiao Huang, Wei Lu, Hongxiang Chen, Xiaolong Chen, An effective approach for the identification of carrier type and local inversion doping in graphene by biased atomic force microscopy, Adv. Electron. Mater. 2 (2016) 1500255.
[29] S. Yu. Davydov, On the electron affinity of silicon carbide polytypes, Semiconductors 41 (2007) 696.
[30] Kaixing Zhu, Liwei Guo, Jingjing Lin, Weichang Hao, Jun Shang, Yuping Jia, et al., Graphene covered SiC powder as advanced photocatalytic material, Appl. Phys. Lett. 100 (2012) 023113.
[31] O. Leenaerts, B. Partoens, F.M. Peeters, Adsorption of H_2O, NH_3, CO, NO_2, and NO on graphene: a first-principles study, Phys. Rev. B 77 (2008) 125416.